Coexistence of Twisted, Plectonemic, and Melted DNA in Small Topological Domains

He Meng, Johan Bosman, Thijn van der Heijden, and John van Noort*
Huygens-Kamerlingh Onnes Laboratory, Leiden University, Leiden, The Netherlands

ABSTRACT DNA responds to small changes in force and torque by over- or undertwisting, forming plectonemes, and/or melting bubbles. Although transitions between either twisted and plectonemic conformations or twisted and melted conformations have been described as first-order phase transitions, we report here a broadening of these transitions when the size of a topological domain spans several kilobasepairs. Magnetic tweezers measurements indicate the coexistence of three conformations at subpicoNewton force and linking number densities ~−0.06. We present a statistical physics model for DNA domains of several kilobasepairs by calculating the full partition function that describes this three-state coexistence. Real-time analysis of short DNA tethers at constant force and torque shows discrete levels of extension, representing discontinuous changes in the size of the melting bubble, which should reflect the underlying DNA sequence. Our results provide a comprehensive picture of the structure of underwound DNA at low force and torque and could have important consequences for various biological processes, in particular those that depend on local DNA melting, such as the initiation of replication and transcription.

INTRODUCTION

In vivo, DNA is maintained in a negatively supercoiled state in small topological domains of several kilobasepairs (kbps) (1,2). This supercoiling forms the driving force for DNA compaction into chromosomes and has been implicated in regulating all processes involving DNA (3). Access to DNA by polymerases, for example, requires melting of a small amount of DNA and may be a rate-limiting step in the initiation of transcription and replication (4). The processive motion of these polymerases in topologically fixed domains can lead to accumulation of force and torque, which has been suggested to play an important role in DNA homeostasis (5–8). It is therefore important to understand how force and torque affect the conformation of DNA.

Using force spectroscopy techniques such as magnetic and optical tweezers, it is possible to control both the force and the torque on single DNA molecules (9–11). Seminal work by Strick et al. (12) showed that under- and overtwisting of DNA leads to plectonemic structures, i.e., supercoils, at stretching forces below 0.5 pN. Above 1.0 pN and negative torque, small dAdT-rich regions of double-stranded(ds)DNA melt and form single-stranded (ss)DNA bubbles (13,14). At higher force ($F > 2.5$ pN) and larger negative torque ($\Gamma < -11$ pN nm), a left-handed structure L-DNA (15) forms. Large positive torque and force, on the other hand, induces a highly overtwisted state called P-DNA (16). Thus, a rich variation of conformations accommodates physical stress and torque in DNA.

Statistical mechanics has been successfully employed to describe these remarkable features of DNA (17,18). In these reports, the DNA tether is assumed to be large enough for neglecting thermal fluctuations between different conformations. For a DNA tether with a finite number of basepairs (i.e., several kbps) held at low forces ($F < 1.2$ pN) and moderate linking number densities ($|\sigma| < 0.06$), representing physiologically relevant conditions (19), coexistence of three states has been suggested (20). However, detailed analysis of the extension of short DNA molecules in this low force and torque range is lacking.

In this article, we provide an extended experimental data set and introduce a numerical three-state model which shows the coexistence of three states in the same topological domain. We performed magnetic tweezers experiments on DNA molecules of several kilobasepairs and measured twist-extension curves in real time. This resolved simultaneously the rather large fluctuations in extension due to the presence of different states, and revealed a discontinuous change in the size of the melting bubbles that we attribute to differences in DNA sequence. Although we do not explicitly take the DNA sequence into account in our statistical physics model, there are indications that suggest that the phase-diagram can be affected by it. Together, these findings provide a quantitative understanding of DNA melting in small topological domains at forces and degrees of supercoiling that are representative for the conditions that occur in the living cell.

MATERIALS AND METHODS

Magnetic tweezers

The home-build magnetic tweezers has been described by Kruithof et al. (21). During an experiment, a DNA molecule was constrained between the end of a superparamagnetic bead with diameter of 1 μm and the surface of a microscope coverslip. Twist was induced by rotating the magnetic field at 1 turn/s. The extension of DNA was measured in real time at a frame rate of 60 Hz with a charge-coupled device camera (Pulnix TM-6710CL; JAI, San Jose, CA).

Submitted October 22, 2013, and accepted for publication January 13, 2014.

*Correspondence: noort@physics.leidenuniv.nl

Editor: Laura Finzi.

0006-3495/14/03/1174/8 $2.00

http://dx.doi.org/10.1016/j.bpj.2014.01.017

DNA constructs

Two DNA constructs were studied based on Plasmid pGem-3Z (3 kb) and Puc18 with 25 repeats of the 601 sequence (8.5 kb) (a gift from D. Rhodes, Singapore). Both plasmids were digested with *Bsa*I and *Bse*YI yielding linear fragments of 2410- and 6960-bp, respectively, with corresponding sticky ends on either side. Digoxigenin and biotin-labeled handles were produced with PCR using biotin-dUTP and digoxigen-dUTP on the pGem-3Z template using the following primers: 5′ GAT AAA TCT GGA GCC GGT GA 3′ and 5′ CTC CAA GCT GGG CTG TGT 3′. After PCR amplification, these fragments were digested with *Bsa*I and *Bse*YI and ligated to the previously digested DNA backbone.

Sample preparation

A clean coverslip was coated with 1% polystyrene-toluene solution. The coverslip was then mounted on a poly-di-methysiloxane (PDMS, Dow Corning, Midland, MI) flow cell containing a 10 × 40 × 0.4 mm flow channel. The flow cell was incubated with 1 μg/mL anti-digoxigenin for 2 h and 2% BSA (w/v) solution overnight. A quantity of 20 ng/mL DNA in 10 mM HEPES pH 7.6, 100 mM KAc, and 10 mM NaN_3 was flushed into the flow cell and incubated for 10 min, followed by flushing in 1-μm streptavidin-coated superparamagnetic microspheres (MyOne; Invitrogen, Carlsbad, CA) in the same buffer after 10 min.

RESULTS

We consider a DNA molecule consisting of N basepairs. When DNA is torsionally unconstrained, the linking number Lk_0 equals 1 helical turn per 10.4 bp (22). In the case of a torsionally constrained molecule, torque builds up as one end of the molecule is twisted ΔLk turns. This change in twist can be expressed in the linking number density, $\sigma \equiv \Delta Lk/Lk_0$. Here, we will examine the situation where three states, i.e., twisted (t), plectonemic (p), and melted (m) DNA occur simultaneously in the same molecule (Fig. 1). In this model, the basepairs in the molecule are divided into these three states,

$$N = n_t + n_p + n_m, \tag{1}$$

where $n_i (i = t, p, m)$ is the number of basepairs in each state. The excess linking number is conserved and distributed between these three states:

$$\Delta Lk = \Delta Lk_t + \Delta Lk_p + \Delta Lk_m. \tag{2}$$

The linking number density in the entire domain can thus be written as

$$\sigma_{\text{tot}} = \frac{n_t}{N}\sigma_t + \frac{n_p}{N}\sigma_p + \frac{n_m}{N}\sigma_m \tag{3}$$

in which σ_i ($i = t, p, m$) is defined as the linking number density in each state ($\sigma_i = \Delta Lk_i/(n_i/10.4)$). The total free energy G equals the sum of the free energy in each state, following

$$G = n_t G_t + n_p G_p + n_m G_m, \tag{4}$$

in which G_i represents the free energy per basepair in state i. In general, G_i can depend on both the force and linking number density (15,17),

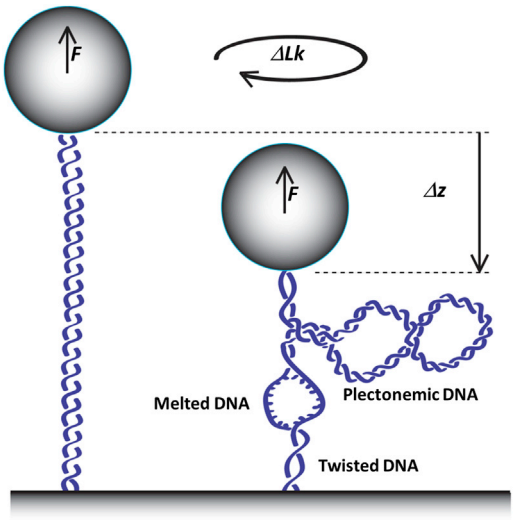

FIGURE 1 Schematic illustration of the conformational changes of a DNA molecule in a magnetic tweezers setup (not to scale). A DNA molecule is tethered between a superparamagnetic bead and a glass surface. Force and torque on the DNA molecule are applied by an external pair of magnets (not shown) to the bead. Here, we consider the coexistence of three states: twisted, plectonemic, and melted DNA. To see this figure in color, go online.

$$G_i(F, \sigma_i) = -g_i(F) + \frac{c_i(F)}{2}(\sigma_i - \sigma_{0,i})^2 + \varepsilon_i, \tag{5}$$

where $g_i(F)$ is the stretching free energy and $c_i(F)$ is the force-dependent twist modulus. For the twisted and melted state, the stretching free energy is described by a wormlike chain (17), whereas stretching of plectonemic DNA is force-independent because it has zero extension. The value $\sigma_{0,i}$ is the degree of twist in each state in absence of torque. The value ε_i is the melting energy for basepair separation, which is zero for twisted and plectonemic DNA. Although the melting energy is sequence-dependent, we will assume an average value of $1.6\,k_BT$ (23) per basepair. All parameters in Eq. 5 are summarized in Table S1 in the Supporting Material.

Previous work by Marko (17) reported an analytical solution for the distribution of states based on equating the torque in each state. In analogy with other phase transitions, only a single point in the phase diagram was reported to represent a three-phase coexistence. However, thermal fluctuations are not negligible in finite systems, such as a single topological domain of several kilobasepairs, allowing for a population of additional states that would remain unobserved in the thermodynamic limit. An analytical solution for such a three-state system has not been reported. Because of the finite number of states, we can numerically calculate the full partition function, using Eqs. 1, 3, and 4. The probability to be in a conformation defined by n_t, n_p, σ_t, and σ_p equals

$$P(F, \sigma_{\text{tot}}) = Z^{-1}\exp\left(\frac{-G(F, \sigma_{\text{tot}}, \sigma_t, \sigma_p, n_t, n_p)}{k_BT}\right), \tag{6}$$

with the partition function

$$Z=\sum_{\sigma_p=-\infty}^{\infty}\sum_{\sigma_t=-\infty}^{\infty}\sum_{n_p=N-n_s}^{N}\sum_{n_s=0}^{N}\exp\left(\frac{-G(F,\sigma_{\mathrm{tot}},\sigma_t,\sigma_p,n_t,n_p)}{k_{\mathrm{B}}T}\right). \tag{7}$$

Using Eq. 4, the extension z of a DNA molecule with contour length L in a state comprising n_t stretched basepairs and n_m melted basepairs becomes

$$\frac{z(F,\sigma_{\mathrm{tot}})}{L}=\frac{n_t}{N}\left(-\frac{\partial G_t}{\partial F}\right)+\frac{n_m}{N}\left(-\frac{\partial G_m}{\partial F}\right). \tag{8}$$

Combining Eqs. 6 and 8 yields for the expected extension

$$\left\langle\frac{z(F,\sigma_{\mathrm{tot}})}{L}\right\rangle=Z^{-1}\sum_{\sigma_p=-\infty}^{\infty}\sum_{\sigma_t=-\infty}^{\infty}\sum_{n_p=N-n_s}^{N}\sum_{n_s=0}^{N}\frac{z(F,\sigma_{\mathrm{tot}})}{L}\exp\left(\frac{-G(F,\sigma_{\mathrm{tot}},\sigma_t,\sigma_p,n_t,n_p)}{k_{\mathrm{B}}T}\right). \tag{9}$$

The mean value and variance of all other parameters that describe the conformation of the molecule are calculated likewise.

Three-state coexistence

We used magnetic tweezers to control the force and twist exerted on a single DNA molecule (Fig. 1). Briefly, the experimental setup consists of a DNA molecule that is anchored between a glass surface and a superparamagnetic bead. The position and the rotation of a pair of external magnets determines the force and twist applied to the bead. The height of the bead, corresponding to the extension of the DNA molecule, is measured in real time using video microscopy and image processing (21). Unlike previous reports (14,24,25), we do not average the extension over a given time interval, so changes in extension are directly revealed. The bandwidth to detect these changes is limited by the viscous drag of the bead, the stiffness of the DNA tether, and the frame rate of the camera (see Fig. S7 in the Supporting Material). Typically, for the conditions of the measurements reported here, fluctuations in extension can be detected at 20–60 Hz. Because each state has a different extension (see Eq. 8), the distribution of states can only be determined indirectly from the total extension of the molecule.

We carried out twisting experiments on 7.0- and 2.4-kbps DNA molecules at forces up to 1.0 pN and linking number densities up to $|\sigma_{\mathrm{tot}}|<0.07$ (Fig. 2 and see Fig. S1 *A* for 7.0 and 2.4 kbps, respectively). Over- and undertwisting the DNA molecule at 0.3 pN resulted in a symmetric decrease in end-to-end distance (Fig. 2, *red circles*). At this force, DNA buckles at both negative and positive torque. The resulting supercoils reduce the end-to-end distance of the DNA molecule. Increasing the force to 1.0 pN results in an asymmetric extension-twist curve (Fig. 2, *blue circles*). The extension remains constant for undertwisting due to DNA melting (13,16,17,26). Overtwisting the DNA creates plectonemes at all forces. The extension at these two conditions can be fully captured by considering the equilibrium between two states: a twisted-melted state or a twisted-plectonemic state (17).

The twist-extension curves at 0.6 and 0.7 pN fall in between these two regimes (Fig. 2, *orange* and *green circles*). We therefore consider the coexistence of twisted, plectonemic, and melted DNA to describe these data. The black lines superimposed on the experimental data in Fig. 2 are the calculations using Eq. 9. The used parameters for the mechanical properties of DNA are summarized in Table S1, using the same values as reported before (17) except for the twist modulus of melted DNA. We could only obtain a good agreement between experimental and simulated data using a twist modulus of melted DNA of 28 nm instead of 1 nm (27). Thus, it appears that small bubbles of melted DNA are more difficult to twist than previously reported.

Note that the model appears to underestimate the extension of the DNA at very small extensions. This is caused by excluded volume forces that originate from the impossibility for the DNA and the bead to penetrate the glass surface (21). We did not correct for this, leading to an underestimation of the effective force for short flexible tethers.

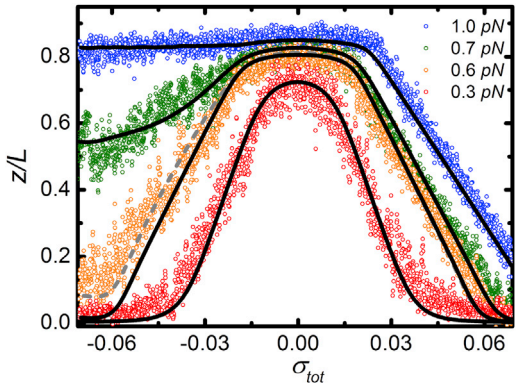

FIGURE 2 Experimental data of the relative extension of a 7.0 kbps DNA molecule as a function of the total linking number density at various forces (*circles*). The relative extension as calculated by Eq. 9 is shown (*lines*). Calculations are based on the parameters summarized in Table S1 in the Supporting Material. (*Solid lines*) Constant melting energy of 1.6 $k_{\mathrm{B}}T$/bp. (*Dashed line*) Force-dependent melting energy (see Fig. S3 *B*), resulting in a better match with the experimental data at 0.6 pN. To see this figure in color, go online.

Barring these deviations at very small extensions, we conclude that under conditions that resemble physiological salt concentrations, the three-state model quantitatively captures experimental twist-extension curves of small topological domains at moderate forces and linking number densities.

Phase diagram

To summarize the distribution of basepairs in the three-state model, we computed a phase diagram of the 7.0-kbps DNA as a function of the linking number density and force (Fig. 3). The fractions of basepairs in each state are color-coded, resulting in separate regions of twisted (*blue*) and plectonemic (*green*) DNA. Several regions show a mixed distribution of two states: twisted and plectonemic DNA (*cyan*), twisted and melted DNA (*pink*), and plectonemic and melted DNA (*yellow*). These features, representing two-state conformations, follow previously reported phase diagrams (9,15,17).

The phase diagram also shows a phase, rather than a single triple point (28), where the three states coexist (*white*). This phase is a direct consequence of the small size of the topological domain, which invalidates the thermodynamic limit assumption and exposes states that are usually obscured in large systems. The phase diagrams for 2.4 and 24.0 kbps DNA (see Fig. S2) reproduce the same trend, but the three-state coexistence regime shrinks when the tether length increases. For 24.0 kbps, we observe only a narrow line at $F = 0.69$ pN. Because of the large difference in linking number between melted DNA and dsDNA, a small melting bubble is more efficient in relieving torsional stress than twisted or plectonemic DNA. In larger tethers, such a small bubble represents a smaller fraction of the total DNA size, reducing the size of the coexistence phase.

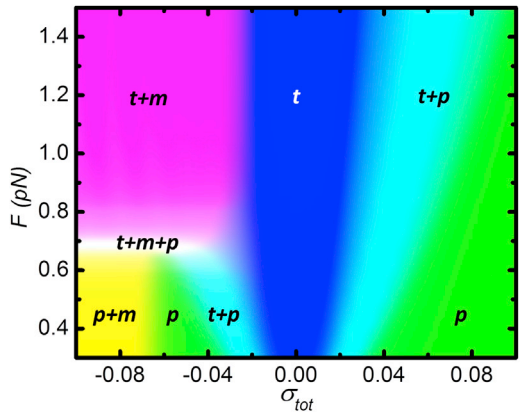

FIGURE 3 The force-linking number density phase diagram of a 7.0-kbps DNA molecule. Gradual transitions occur between twisted (*t*), plectonemic (*p*), and melted (*m*) DNA. (*Blue*, *green*, and *red*) The fraction of basepairs in *t*, *p*, and *m*, respectively. The fraction of melted bps was multiplied by 10 in all regions to optimize the contrast. (*White region*) Three-state coexistence phase. To see this figure in color, go online.

To better understand the three-state coexistence, we looked into more details that can be calculated with the statistical mechanics model. Fig. 4 *A* shows the number of basepairs in the three states for 7.0 kbps DNA at $F = 0.7$ pN. The majority of the DNA is in the twisted state for $|\sigma_{tot}| < 0.04$. For $|\sigma_{tot}| > 0.01$, plectonemic DNA starts to form, whereas at $\sigma_{tot} < -0.02$, melted DNA is formed. A small fraction of the DNA contributes to this melting bubble, though it grows to 250 bps for $\sigma_{tot} = -0.07$.

Although only a small fraction of the DNA molecule melts, these basepairs contribute to a large part of the total twist that is present in the DNA tether. Fig. 4 *B* shows the distribution of excess linking number among the three states. At small linking number densities, all the twist is absorbed in twisted DNA. When σ_{tot} in the DNA molecule exceeds 0.02, the molecule buckles, and the additional twist is stored in plectonemes. For negative torque, however, at $\sigma_{tot} < -0.04$ most of the twist is stored in melted DNA. The large difference in helicity and free energy between dsDNA and melted DNA makes melted DNA a good buffer for torsional stress.

We extended our analysis to the quantification of torque within a 7.0-kbps DNA molecule for different forces and linking number densities (see the Fig. S4, and Fig. 4 *C*). Fig. 4 *C* shows that the torque increases linearly with twist when DNA exists in a single state. For example, the plectonemic state dominates at $F = 0.1$ pN and $\sigma_{tot} > -0.05$ (with a small interruption at $\sigma_{tot} = 0$). Under these conditions, the slope represents the twist stiffness of plectonemic DNA. At larger forces and small twist densities, DNA is predominantly twisted, yielding a larger slope because of the larger twist persistence length of twisted DNA. When multiple states coexist, an increase of torsional stress is accommodated by a redistribution of the states rather than increasing the twist in either of the states. Thus, for mixed conformations, the torque stays constant but the distribution of basepairs between states is shifted (Fig. 4 *A*). Remarkably, the negative torque reaches a minimum value of -11 pN nm for all forces probed. This torque corresponds to a free energy of 2.6 k_BT, which is just sufficient to melt and twist an additional basepair. Thus, the maximum torque for negatively twisted DNA is limited. As a consequence, the linking number density in the plectonemic state, which comprises most of the DNA, is constrained, i.e., $\langle \sigma_p \rangle = -0.065$, in excellent agreement with the natural linking number density observed in vivo (19,29).

The model presented here differs from previous work in two aspects (17):

1. We consider the distribution of all states, rather than only the lowest energy state. In small tethers, there is a large number of states with a comparable free energy contributing to the average extension of the molecule. Fig. 4 *D* shows the expected value and standard deviation of n_m as a function of the applied linking number density

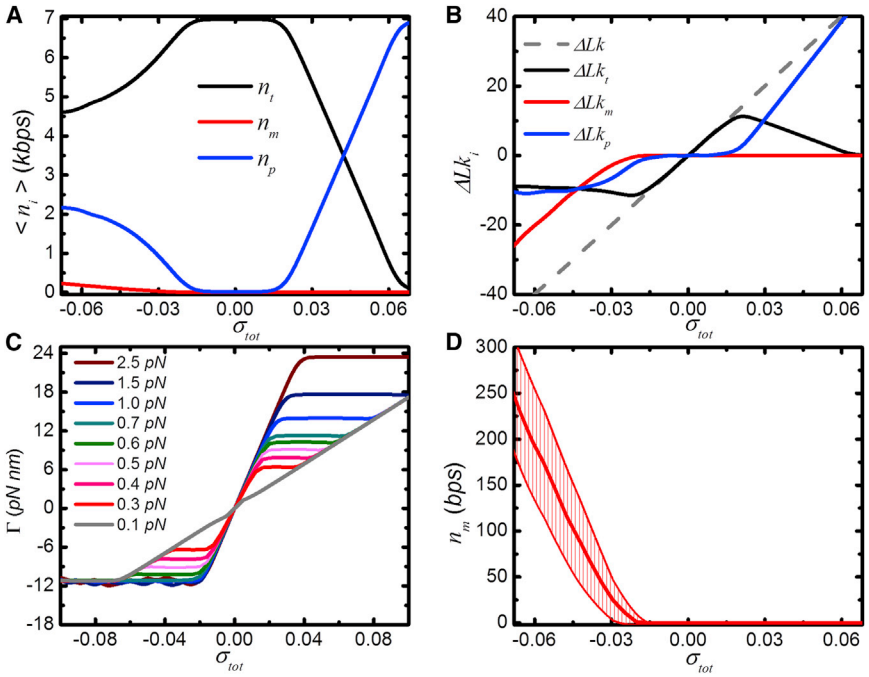

FIGURE 4 Calculations of the three-state coexistence in a 7.0-kbps DNA molecule at 0.7 pN and different linking number densities. (*A*) The distribution of basepairs in each state. (*B*) The distribution of linking numbers in each state. The sum of linking numbers converges to the total linking number ΔLk (*shaded*). (*C*) The torque present in the DNA molecule calculated between 0.1 and 2.5 pN. (*D*) The distribution of melted basepairs. (*Error bars*) Standard deviation. To see this figure in color, go online.

calculated. It is clear from these calculations that the bubble size is not well defined, with variations ranging up to 50 bps, emphasizing the extent of the statistical fluctuations in a small DNA tether.

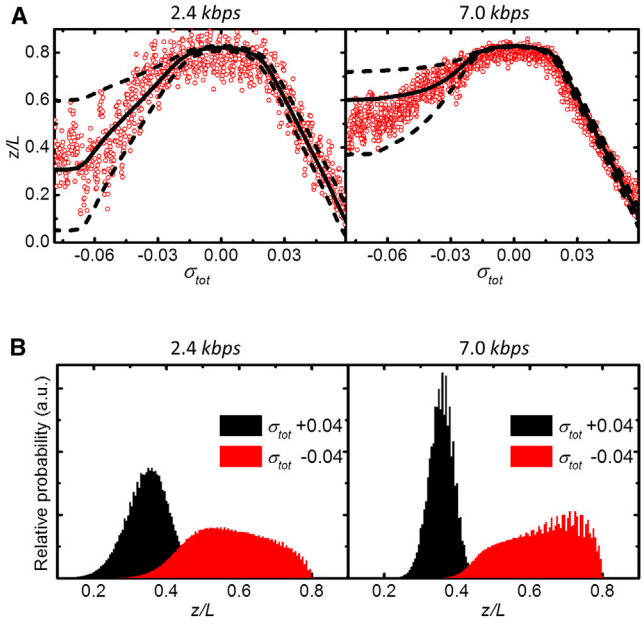

FIGURE 5 (*A*) Experimental data of the relative extension versus linking number density (*red circles*) at 0.7 pN for 2.4 kbps (*left*) and 7.0 kbps DNA (*right*). (*Solid black line*) Calculated median extension value. (*Dashed lines*) 68% range in extension. (*B*) Calculated extension distribution for 2.4 kbps (*left*) and 7.0 kbps DNA (*right*) at $\sigma_{tot} = -0.04$ (*red*) and $\sigma_{tot} = +0.04$ (*black*). Note the broad and asymmetric extension distribution compared to the Gaussian profile for negative and positive twist, respectively. To see this figure in color, go online.

2. The torque is not fixed within the molecule. As shown in Fig. S4, the mean values of the torque in each phase follow the mean torque of the entire molecule, but significant variations in torque occur when phases coexist. Imposing a constant torque throughout the entire molecule still results in the coexistence of three states (see Fig. S5). Fluctuations in torque between the different parts of the molecule therefore only contribute a small part of the states that define the average extension.

Fluctuations in extension

The relatively broad distribution of basepairs in each of the three states results in increased fluctuations in the extension of the molecule, due to the large differences in extension between the three states. Indeed, closer inspection of the extension-twist curves as shown in Fig. 2 reveals increased fluctuations in the extension in the three-state coexistence region. In these experiments, the data were not time-averaged, revealing independent extension measurements while twisting the DNA molecule. The magnitude of these fluctuations can be calculated using Eqs. 6 and 8. Fig. 5 *A* shows twist-extension measurements of a 2.4- and a 7.0-kbps DNA molecule along with the calculated median and variation in extension at $F = 0.7$ pN. The latter was calculated as the range that includes 68% of the extension distribution. Due to the variations among the three states, the extension is not Gaussian-distributed for undertwisting as opposed to overtwisting (Fig. 5 *B* and see Fig. S6 *B*), but displays an asymmetric distribution. The fluctuations caused by transitions between different states dominate

over thermal fluctuations in extension that are always present in flexible polymers, as discussed in the Supporting Material. Overall, we obtain a fair agreement between the calculated magnitude of the fluctuations in extension and experimental data. This shows that the increased fluctuations in extension at undertwisting conditions can be attributed to transitions between different conformations of the molecule.

Fluctuations in extension at constant force and linking number measured in real time (Fig. 6) uniquely reveal the kinetics of the transitions between different states in the molecule. Such kinetics cannot be obtained from the statistical mechanics model presented here, which only describes the equilibrium situation. Remarkably, we observed distinct transitions between discrete levels (~110 nm) of extension of the molecule in the three-state coexistence regime. Because the twisted and melted DNA have a comparable extension in this force regime, the discrete extension levels can only be explained by changes in the size of the plectoneme. Our model suggests the extension levels correspond to changes of ~400 bps of plectonemic DNA transferring back and forth into 380-bps twisted and 20-bps melted DNA. The transitions occur at intervals of several seconds. We attribute the discrete levels in extension to barriers originating from differences in the sequence of the DNA. Small stretches of GC basepairs, having one more hydrogen bond than AT basepairs, present a kinetic barrier for extension of the melting bubble. Such inhomogeneities will severely change the distribution and kinetics of the molecule's extension. For bubbles spanning several tens of basepairs, this results in a limited number of favored states, depending on the local DNA sequence.

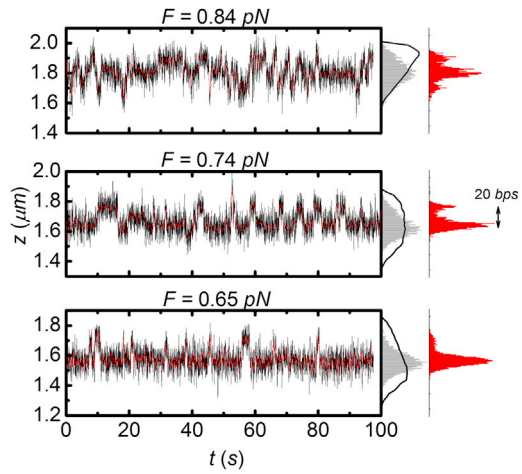

FIGURE 6 Constant force measurements at a linking number density $\sigma_{tot} = -0.03$. Three different forces are shown (*top to bottom*): 0.84, 0.74, and 0.65 pN. (*Red*) The 20 points of median filtered data, emphasizing the discrete transitions in extension. Histograms of the extension are shown on the right side of the time traces (*black* and *red bars*). The calculated extension distribution is superimposed on the histogram (*solid black lines*). The discrete levels are attributed to ~400 bps of plectonemic DNA transferring back and forth into 380-bps twisted and 20-bps melted DNA. To see this figure in color, go online.

We noted that the shape of the twist-extension curves is salt-dependent (see Fig. S1). Increasing the ionic strength from 100 to 300 mM KAc shifts the twist-extension curves to smaller extensions for undertwisting. This is consistent with the well-known increase of the melting energy for DNA at higher salt concentrations (23), as also observed for force-induced melting without twist (30). Increasing the melting energy from 1.6 to 2.0 k_BT per basepair recovered a good agreement between experimental and calculated data.

Although in principle it should be straightforward to extend the current three-state model with a sequence-dependent melting energy, such calculations will require large computational effects, even for small molecules. It is important to note that this sequence heterogeneity can have a significant effect on the phase diagram. We expect that small melting bubbles will preferably be formed in AT-rich regions, but as the force increases, such AT-rich regions will expand into GC-rich parts at their boundaries. We modeled this increased contribution of GC basepairs by increasing the melting energy in a linear fashion from 1.5 to 2.1 k_BT for forces between 0.6 and 1.2 pN. For $F =$ 0.6 pN, the adjusted twist extension curves show a small increase in extension at negative twist (Fig. 2, *gray dashed line*), yielding a better agreement with the experimental data (see Fig. S1 *A*; *dashed lines* = 2.4 kbps DNA). The resulting phase diagram is globally similar to that presented in Fig. 3, but displays a larger area in which the three states coexist (see Fig. S3). Thus, although the sequence dependence of melting bubbles is not included explicitly in our model, the data give clear indications that there is a significant effect of sequence heterogeneity, resulting in both discrete, 20-bp steps in the size of the melting bubble and in a larger area in which the three states coexist.

DISCUSSION AND CONCLUSIONS

We described the coexistence of twisted, plectonemic, and melted DNA in small topological domains. Using a numerical three-state model, we computed a force-twist phase diagram that reproduces earlier descriptions of supercoiled DNA. However, we observe gradual transitions and a region of three-state coexistence rather than a sharp first-order phase transition and a single triple point. DNA melting induced by large forces is well studied in recent works (31–34), including the effect of torque (9,15). Here we studied these effects at low forces and moderate linking number densities. This situation is particularly relevant in vivo, where topological domains are likely to be several kilobasepairs, forces are not likely to exceed several picoNewtons, and linking number densities are generally close to −0.06. Moreover, we computed that melting bubbles of several tens of basepairs appear in such a domain.

The continuous presence and the large dynamics of such bubbles may have important consequences for processes involving ssDNA.

Sheinin et al. (15) showed that long stretches of melted DNA are organized in a L-DNA structure with $\langle\sigma_m\rangle = -1.8$, corresponding with a helical repeat of ~13 bp/turn, and a twist modulus of 20 nm. They also observed that the torque in undertwisted DNA is limited to −11 pN nm under extreme twist densities of σ_{tot} down to −2.0 and $F > 5$ pN. We show here that also under less extreme conditions, this torque limit applies. Strick et al. (13,14) reported that melted DNA remains in a disordered conformation resembling two strands of ssDNA with $\langle\sigma_m\rangle = -1$. The twist modulus of a DNA bubble was considered very small, ~1 nm. We obtained the best agreement between experimental and simulated data for $\langle\sigma_m\rangle = -1.05$ and a twist modulus of 28 nm. This may indicate that small melting bubbles are more difficult to twist than long ssDNA molecules and may point to alternative interactions between the melted bases that are not present in larger stretches of melted DNA. Further studies are required to reveal possible structure in small melting bubbles.

It is clear that the finite size of the melting bubble and the large impact of sequence inhomogeneities have a significant effect on the twist-extension curves of DNA. From our studies, we cannot resolve the position of the bubble. A melting bubble could for example be positioned at the tip of the plectoneme, rather than in the twisted section of the DNA. Such a melting bubble in the plectonemic region would not lead to an increase of the extension, relative to plectonemic DNA, but would reduce the torsional stress. DNA sequence may also result in highly curved DNA stretches that could localize the plectoneme at specific locations. The good agreement of the experimental data with a simple three-state statistical physics model that does not include sequence effects suggests that such dependencies only play a minor role.

One of the most remarkable findings is that distinct steps in extension of the DNA molecule are clearly visible under small force and negative torque. Such steps can easily be confused with protein-induced changes in extension when studying protein-DNA interactions. Because long DNA substrates, such as λ-DNA with a contour length of 48 kbps, are generally replaced by shorter DNA molecules in more recent studies, the presence of bubble-plectoneme transitions may be relevant for many force-spectroscopy studies.

The lifetime of the distinct levels of DNA extension (Fig. 6) that we attribute to DNA melting are much longer than the lifetime of melting bubbles obtained from fluorescence correlation spectroscopy (FCS) measurements, i.e., ~50 μs (35). This may be due to the force that is applied in the magnetic tweezers, which is absent in FCS. Moreover, the melting bubbles described here may be larger than those captured in the FCS experiments. We cannot exclude the presence of very short-lived states, because of the limited response time of the bead-tether mechanics.

The simulations are amendable for further refinements. In addition to introducing a sequence-dependent melting energy, which may resolve the discrete levels of extension, one can include an entropic penalty for the formation of a melting bubble (26). Similarly, a penalty may be included for the formation of a DNA buckle (36–38). Without such penalties, we do not discriminate between single or multiple domains within one DNA molecule. More advanced modeling of overtwisted DNA, which includes electrostatic interactions between DNA segments, suggests that the formation of multiple plectonemes or melting bubbles in the same topological domain may have a significant effect on twist-extension curves (18). However, experiments show that small molecules at moderate force and torque only feature single domains of bubbles and plectonemes (39,40). Although this indicates that the free energy for formation of a new domain exceeds that of the free energy increase per basepair, it may be relatively small compared to the total free energy of the entire domain. Therefore, Eq. 4 will be adequate for describing the different conformations of a small DNA tether.

In summary, our work resolved and quantitatively described the coexistence of three different states in DNA. This fresh insight may have implications for the interaction mechanism of proteins that interact with DNA in torsionally constraint domains, such as topoisomerases, transcription factors, histones, and DNA-based molecular motors such as DNA and RNA polymerases and chromatin remodelers.

SUPPORTING MATERIAL

One table, six equations, seven figures and References (41–43) are available at http://www.biophysj.org/biophysj/supplemental/S0006-3495(14)00087-3.

We thank J. F. Marko, B. Eslami-Mossallam, H. Schiessel, and K. Andresen for stimulating discussions and helpful suggestions.

H.M. was supported by the Human Frontier Science Program.

REFERENCES

1. Champoux, J. J. 2001. DNA topoisomerases: structure, function, and mechanism. *Annu. Rev. Biochem.* 70:369–413.

2. Postow, L., C. D. Hardy, …, N. R. Cozzarelli. 2004. Topological domain structure of the *Escherichia coli* chromosome. *Genes Dev.* 18:1766–1779.

3. Pruss, G. J., and K. Drlica. 1989. DNA supercoiling and prokaryotic transcription. *Cell.* 56:521–523.

4. Murakami, K. S., S. Masuda, …, S. A. Darst. 2002. Structural basis of transcription initiation: an RNA polymerase holoenzyme-DNA complex. *Science.* 296:1285–1290.

5. Postow, L., B. J. Peter, and N. R. Cozzarelli. 1999. Knot what we thought before: the twisted story of replication. *BioEssays.* 21:805–8.

6. Revyakin, A., C. Liu, …, T. R. Strick. 2006. Abortive initiation and productive initiation by RNA polymerase involve DNA scrunching. *Science.* 314:1139–1143.
7. Kurth, I., R. E. Georgescu, and M. E. O'Donnell. 2013. A solution to release twisted DNA during chromosome replication by coupled DNA polymerases. *Nature.* 496:119–122.
8. Ma, J., L. Bai, and M. D. Wang. 2013. Transcription under torsion. *Science.* 340:1580–1583.
9. Bryant, Z., M. D. Stone, …, C. Bustamante. 2003. Structural transitions and elasticity from torque measurements on DNA. *Nature.* 424:338–341.
10. Deufel, C., S. Forth, …, M. D. Wang. 2007. Nanofabricated quartz cylinders for angular trapping: DNA supercoiling torque detection. *Nat. Methods.* 4:223–225.
11. Lipfert, J., J. W. J. Kerssemakers, …, N. H. Dekker. 2010. Magnetic torque tweezers: measuring torsional stiffness in DNA and RecA-DNA filaments. *Nat. Methods.* 7:977–980.
12. Strick, T. R., J. F. Allemand, …, V. Croquette. 1996. The elasticity of a single supercoiled DNA molecule. *Science.* 271:1835–1837.
13. Strick, T. R., V. Croquette, and D. Bensimon. 1998. Homologous pairing in stretched supercoiled DNA. *Proc. Natl. Acad. Sci. USA.* 95:10579–10583.
14. Strick, T. R., J. F. Allemand, …, V. Croquette. 1998. Behavior of supercoiled DNA. *Biophys. J.* 74:2016–2028.
15. Sheinin, M. Y., S. Forth, …, M. D. Wang. 2011. Underwound DNA under tension: structure, elasticity, and sequence-dependent behaviors. *Phys. Rev. Lett.* 107:108102.
16. Allemand, J. F., D. Bensimon, …, V. Croquette. 1998. Stretched and overwound DNA forms a Pauling-like structure with exposed bases. *Proc. Natl. Acad. Sci. USA.* 95:14152–14157.
17. Marko, J. F. 2007. Torque and dynamics of linking number relaxation in stretched supercoiled DNA. *Phys. Rev. E Stat. Nonlin. Soft Matter Phys.* 76:021926.
18. Emanuel, M., G. Lanzani, and H. Schiessel. 2013. Multiplectoneme phase of double-stranded DNA under torsion. *Phys. Rev. E Stat. Nonlin. Soft Matter Phys.* 88:022706.
19. Lee, D. H., and R. F. Schleif. 1989. In vivo DNA loops in araCBAD: size limits and helical repeat. *Proc. Natl. Acad. Sci. USA.* 86:476–480.
20. Salerno, D., A. Tempestini, …, F. Mantegazza. 2012. Single-molecule study of the DNA denaturation phase transition in the force-torsion space. *Phys. Rev. Lett.* 109:118303.
21. Kruithof, M., F. Chien, …, J. van Noort. 2008. SubpicoNewton dynamic force spectroscopy using magnetic tweezers. *Biophys. J.* 94:2343–2348.
22. Wang, J. C. 1979. Helical repeat of DNA in solution. *Biochemistry.* 76:200–203.
23. Schildkraut, C., and S. Lifson. 1965. Dependence of the melting temperature of DNA on salt concentration. *Biopolymers.* 3:195–208.
24. Lipfert, J., S. Klijnhout, and N. H. Dekker. 2010. Torsional sensing of small-molecule binding using magnetic tweezers. *Nucleic Acids Res.* 38:7122–7132.
25. Shao, Q., S. Goyal, …, D. Dunlap. 2012. Physiological levels of salt and polyamines favor writhe and limit twist in DNA. *Macromolecules.* 45:3188–3196.
26. Jeon, J. H., and W. Sung. 2008. How topological constraints facilitate growth and stability of bubbles in DNA. *Biophys. J.* 95:3600–3605.
27. Kahn, J. D., E. Yun, and D. M. Crothers. 1994. Detection of localized DNA flexibility. *Nature.* 368:163–166.
28. Marko, J. F. 2009. Mathematics of DNA Structure, Function and Interactions, Vol. 150, The IMA Volumes in Mathematics and its Applications. C. J. Benham, S. Harvey, W. K. Olson, D. W. Sumners, and D. Swigon, editors. Springer, New York, pp. 225–249.
29. Goldstein, E., and K. Drlica. 1984. Regulation of bacterial DNA supercoiling: plasmid linking numbers vary with growth temperature. *Proc. Natl. Acad. Sci. USA.* 81:4046–4050.
30. Huguet, J. M., C. V. Bizarro, …, F. Ritort. 2010. Single-molecule derivation of salt dependent base-pair free energies in DNA. *Proc. Natl. Acad. Sci. USA.* 107:15431–15436.
31. Gross, P., N. Laurens, …, G. J. L. Wuite. 2011. Quantifying how DNA stretches, melts and changes twist under tension. *Nat. Phys.* 7:731–736.
32. Zhang, X., H. Chen, …, J. Yan. 2012. Two distinct overstretched DNA structures revealed by single-molecule thermodynamics measurements. *Proc. Natl. Acad. Sci. USA.* 109:8103–8108.
33. Zhang, X., H. Chen, …, J. Yan. 2013. Revealing the competition between peeled ssDNA, melting bubbles, and S-DNA during DNA overstretching by single-molecule calorimetry. *Proc. Natl. Acad. Sci. USA.* 110:3865–3870.
34. King, G. A., P. Gross, …, E. J. G. Peterman. 2013. Revealing the competition between peeled ssDNA, melting bubbles, and S-DNA during DNA overstretching using fluorescence microscopy. *Proc. Natl. Acad. Sci. USA.* 110:3859–3864.
35. Altan-Bonnet, G., A. Libchaber, and O. Krichevsky. 2003. Bubble dynamics in double-stranded DNA. *Phys. Rev. Lett.* 90:138101.
36. Forth, S., C. Deufel, …, M. D. Wang. 2008. Abrupt buckling transition observed during the plectoneme formation of individual DNA molecules. *Phys. Rev. Lett.* 100:148301.
37. Brutzer, H., N. Luzzietti, …, R. Seidel. 2010. Energetics at the DNA supercoiling transition. *Biophys. J.* 98:1267–1276.
38. Marko, J. F., and S. Neukirch. 2012. Competition between curls and plectonemes near the buckling transition of stretched supercoiled DNA. *Phys. Rev. E Stat. Nonlin. Soft Matter Phys.* 85:011908.
39. van Loenhout, M. T. J., M. V. de Grunt, and C. Dekker. 2012. Dynamics of DNA supercoils. *Science.* 338:94–97.
40. Jeon, J.-H., J. Adamcik, …, R. Metzler. 2010. Supercoiling induces denaturation bubbles in circular DNA. *Phys. Rev. Lett.* 105:208101.
41. Marko, J. F., and E. D. Siggia. 1995. Stretching DNA. *Macromolecules.* 28:8759–8770.
42. Neuman, K. C., and A. Nagy. 2008. Single-molecule force spectroscopy: optical tweezers, magnetic tweezers and atomic force microscopy. *Nat. Methods.* 5:491–505.
43. De Vlaminck, I., T. Henighan, …, C. Dekker. 2012. Magnetic forces and DNA mechanics in multiplexed magnetic tweezers. *PLoS ONE.* 7:e41432.

SUPPORTING MATERIAL

Coexistence of twisted, plectonemic, and melted DNA in small topological domains

He Meng, Johan Bosman, Thijn van der Heijden, John van Noort

Parameters used in the 3 state model

The free energy per base pair in each state follows a parabolic function in σ [1, 2]:

$$G_i(F, \sigma_i) = -g_i(F) + \frac{c_i(F)}{2}(\sigma_i - \sigma_{0,i})^2 + \varepsilon_i,$$

where i denotes the twisted (t), plectonemic (p), or melted (m) state. The values of the individual parameters are shown in Table S1:

Table S1: The force and torque dependent descriptions for the free energy of the 3 state model

	$g_i(F)$	$c_i(F)$	$\sigma_{0,i}$	$\varepsilon_i(k_BT/bp)$	$A_i\,(nm)$	$C_i\,(nm)$
t	$F - \sqrt{k_BT \cdot F/A_t}$	$k_BT\omega_0^2 \cdot C_t\left[1 - \frac{C_t}{4A}\left(\frac{k_BT}{AF}\right)\right]$	0	0	50	100
p	0	$k_BT\omega_0^2 \cdot C_p$	0	0	0	24
m	$1.2(F - \sqrt{k_BT \cdot F/A_m})$	$k_BT\omega_0^2 \cdot C_m$	-1	1.6	4	28

A_i and C_i are the persistence length and twist modulus. $\omega_0 = 2\pi/3.6\,nm = 1.75\,nm^{-1}$, is the inverted pitch of the double helix. All parameters used are the same as [1, 2], except for the twist modulus of melted DNA.

Torque calculation

The torque was calculated separately for each state. The torque is defined as

$$\Gamma_i = \frac{1}{\omega_0}\frac{\partial G_i}{\partial \sigma_i} = k_BT\omega_0 \cdot C_i(\sigma_i - \sigma_{0,i}). \tag{1}$$

The mean torque is calculated as:

$$< \Gamma >= \frac{\sum\limits_{i=t,\,p,\,m} n_i\Gamma_i}{N}. \tag{2}$$

Fluctuations in extension

In Fig. S6 A, we plot the calculated standard deviations (SD) in the extension of a $7.0\,kbps$ DNA molecule from experimental and modeled data (colored and dashed lines, respectively) as a function of the force applied at different linking number densities. Transitions between states are not the only cause of fluctuations in the experimental twist-extension curves. Thermal fluctuations due to the low stiffness of the tether also contribute. Such thermal noise was not included in Fig. 5 A. The magnitude of these fluctuations can be calculated using the equipartition theorem:

$$SD_{thermal} = \sqrt{k_B T / k_z}, \tag{3}$$

where k_z equals $\frac{\partial F}{\partial z}$. In the case of a worm-like chain[3]:

$$k_z = \frac{k_B T}{AL}(1 + \frac{1}{2(1 - \frac{z}{L})^3}). \tag{4}$$

In Fig. S6 A the SD in the extension caused by thermal fluctuations is shown as gray dashed lines. The SD by our 3-state model is obtained by

$$SD_{statistical} = \sqrt{< (\frac{z}{L})^2 > - < \frac{z}{L} >^2}. \tag{5}$$

The black dashed line in Fig. S6 A shows the SD at $\sigma_{tot} = -0.045$. For $F > 1.2\,pN$, where only two states coexist, the experimental data largely follow the thermal fluctuations of the molecule. Between 0.6 and 1.0 pN, we observe increased fluctuations due to the coexistence of the three states. We observe the same trends in the experimental and calculated data, though the amplitude of the fluctuations in the experimental data sometimes exceeds the predicted amplitude.

Some reduction of the fluctuations in extension can be attributed to the slow response time of the bead or to the limited frame rate of the camera. The temporal resolution in the extension is calculated from the corner frequency f_c[4].

$$f_c = \frac{k_z}{12\pi^2 \eta R}. \tag{6}$$

The results calculated for a 7.0 *kbps* DNA molecule are shown in Fig. S7 (black line) using a viscosity $\eta = 1.0 \times 10^{-3}\,Pa\,s$, and a radius of the magnetic bead $R = 0.5\,\mu m$.Imperfect alignment of the magnetic field with the optical axis of the microscope results in small oscillations in extension when the external magnets of the tweezers are rotated[5]. This artifact can be omitted by following the extension of the tether at a fixed linking number.

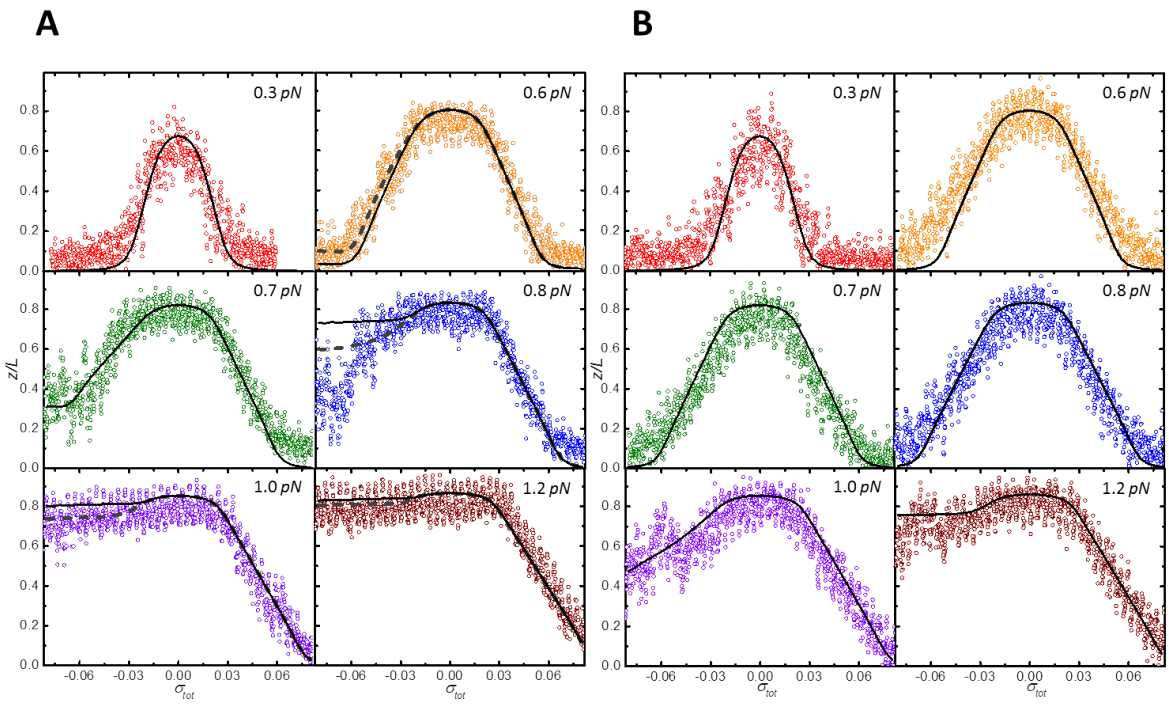

Figure S1

The relative extension as a function of the linking number density of a 2.4 *kbps* DNA molecule in (A) 100 mM KAc at various forces (colored circles). The relative extension as calculated by the numerical model is shown as black solid lines. The dashed lines are the theoretical results for a melting energy that increases linearly with force between $\varepsilon_m = 1.5\,k_BT$ at 0.6 pN to $\varepsilon_m = 2.1\,k_BT$ at 1.2 pN. Such a force dependent melting energy results in a better overlap with the experimental data. (B) Same experiments at 300 mM KAc (colored circles). The relative extension as calculated by the numerical model is shown as black solid lines using a melting energy of $2.0\,k_BT/bp$.

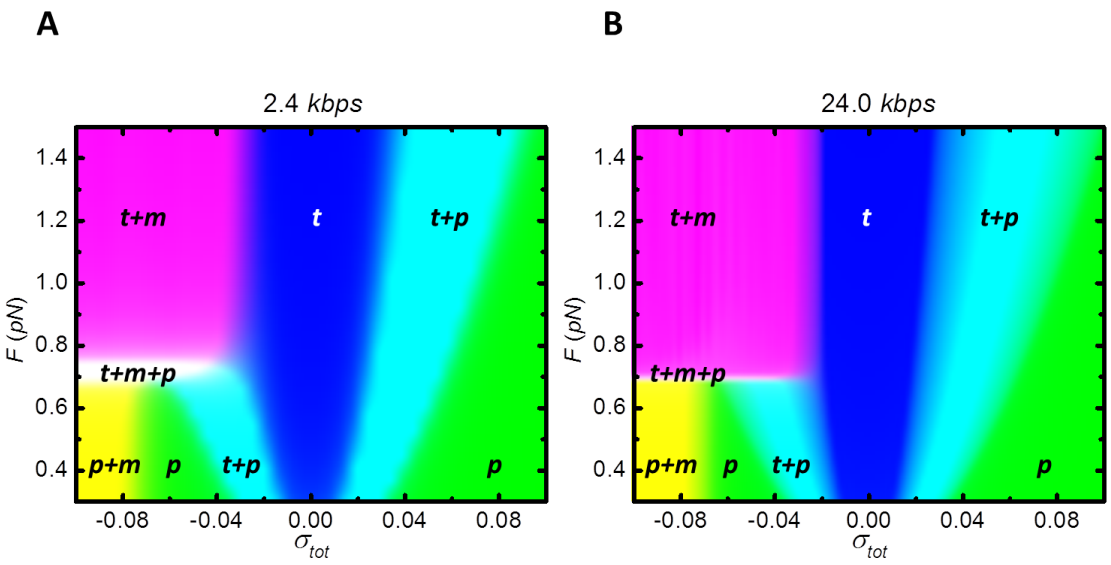

Figure S2

Force-linking number density phase diagrams. (A) A 2.4 *kbps* DNA molecule shows transitions between extended twist-extended (t), plectonemic (p), and melted (m) DNA results, (B) A 24.0 *kbps* DNA molecule shows the same trend as 2.4 *kbps* DNA but a highly reduced 3-state coexistence region.

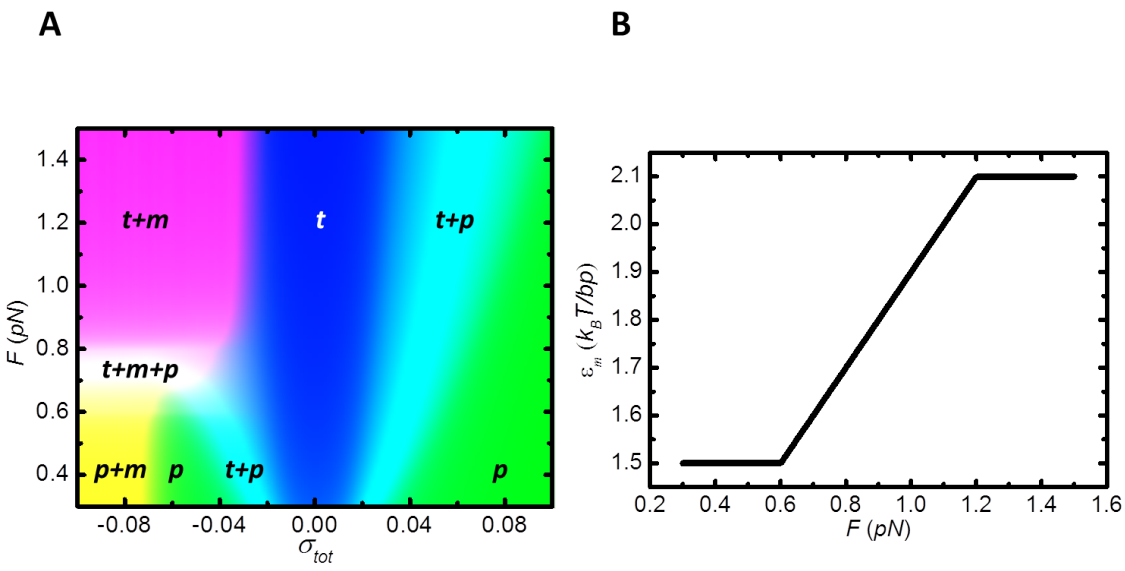

Figure S3

(A) The force linking number density phase diagram of a 7.0 *kbps* DNA with a force dependent free melting energy. (B) The melting energy as a function of the applied stretching force as used for computing the density phase diagram in (A).

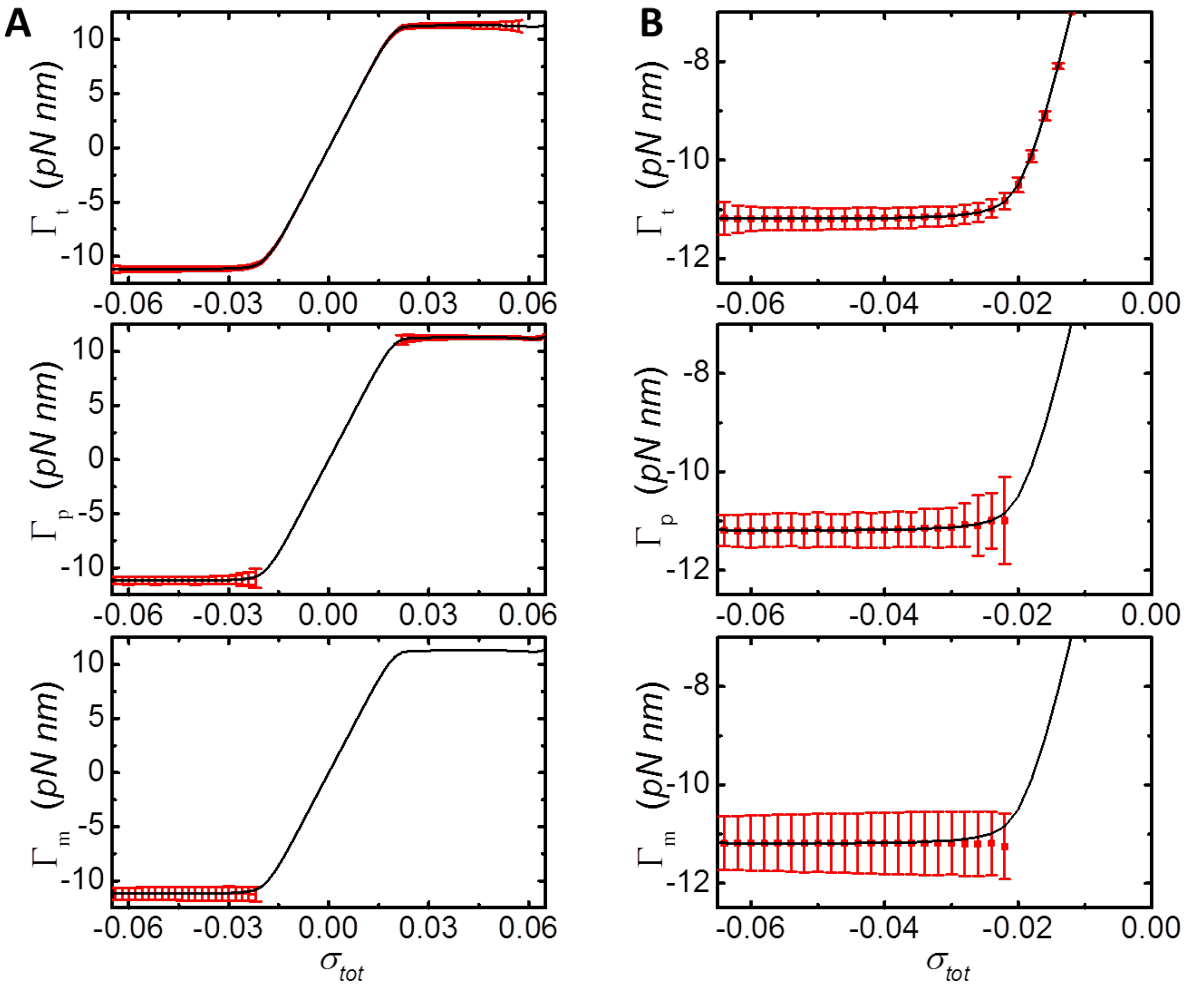

Figure S4

The torque distribution in each state of a 7.0 *kbps* DNA molecule at 0.7 pN. (A) The black line is the average torque in the molecule, whereas the red dots with their respective error bars represent the torque and its standard deviation in each of the occupied states. When the corresponding state is not occupied, the red dots are not shown. (B) Zoom in for a negative linking number density showing significant variations in the torque while the 3-state coexistence region is occupied.

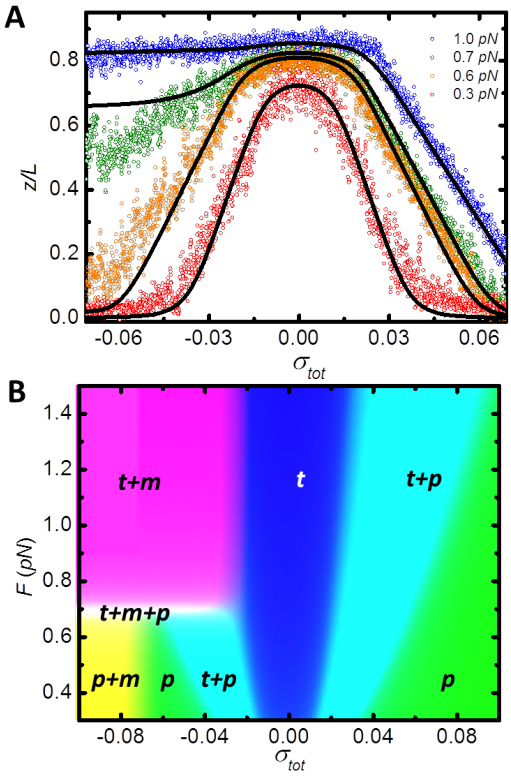

Figure S5

Torque-fixed calculation results of a 7.0 *kbps* DNA molecule. (A) The relative extension as calculated by the numerical model with a constant torque throughout the molecule as black solid lines, compared with experimental data. (B) Force-linking number density phase diagram.

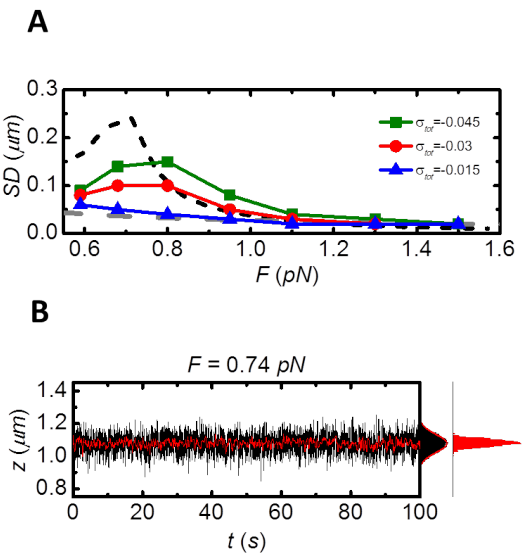

Figure S6

(A) Experimental data of the standard deviation of the extension of a 7.0 *kbps* DNA molecule at different linking number densities with respect to the force applied. Data show increased fluctuations in extension at 0.7 pN. Fluctuations in the extension calculated based on thermal fluctuations only (gray dashed line) cannot capture this effect. SD calculated with the 3-state model (black dashed line) at $\sigma_{tot} = -0.045$ shows however a similar trend. (B) Constant force measurement of a 7.0 *kbps* DNA molecule at $\sigma_{tot} = +0.03$. The red data is the 20 points median filtered data which do not reveal discrete steps as observed for negative linking number densities (Fig. 6). Histograms of the extension are shown on the right side of time traces (black and red bars). The raw data histogram is well fit by a Gaussian (red solid lines).

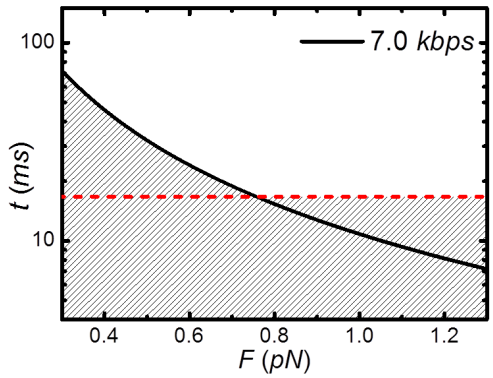

Figure S7

The temporal resolution of the experimental setup at different stretching forces. The black solid line represents the response time of a 7.0 *kbps* DNA molecule as calculated by Equation 6. The red solid line represents the frame rate of the CCD camera used. The shadowed region denotes the dynamics which cannot be resolved in this experiment.

Supporting References

[1] Marko, J. 2007. Torque and dynamics of linking number relaxation in stretched supercoiled DNA. *Physical Review E.* 76:021926.

[2] Sheinin, M. Y., S. Forth, J. F. Marko, and M. D. Wang. 2011. Underwound DNA under Tension: Structure, Elasticity, and Sequence-Dependent Behaviors. *Physical Review Letters.* 107:108102.

[3] Marko, J. F., and E. D. Siggia. 1995. Stretching DNA. *Macromolecules.* 28:8759–8770.

[4] Neuman, K. C., and A. Nagy. 2008. Single-molecule force spectroscopy : optical tweezers , magnetic tweezers and atomic force microscopy. *Nature methods.* 5:491–505.

[5] De Vlaminck, I., T. Henighan, M. T. J. van Loenhout, D. R. Burnham, and C. Dekker. 2012. Magnetic forces and DNA mechanics in multiplexed magnetic tweezers. *PloS one.* 7:e41432.